JPE 16-2-34

http://dx.doi.org/10.6113/JPE.2016.16.2.760
ISSN(Print): 1598-2092 / ISSN(Online): 2093-4718

A New Islanding Detection Method Based on Feature Recognition Technology

Xinxin Zheng*, Lan Xiao†, Wenwen Qin*, and Qing Zhang*

*New Energy Automobile Engineering Research Institute, Hefei University of Technology, Anhui, China
†Automation College, Nanjing University of Aeronautics and Astronautics, Jiangsu, China

Abstract

Three-phase grid-connected inverters are widely applied in the fields of new energy power generation, electric vehicles and so on. Islanding detection is necessary to ensure the stability and safety of such systems. In this paper, feature recognition technology is applied and a novel islanding detection method is proposed. It can identify the features of inverter systems. The theoretical values of these features are defined as codebooks. The difference between the actual value of a feature and the codebook is defined as the quantizing distortion. When islanding happens, the sum of the quantizing distortions exceeds the threshold value. Thus, islanding can be detected. The non-detection zone can be avoided by choosing reasonable features. To accelerate the speed of detection and to avoid miscalculation, an active islanding detection method based on feature recognition technology is given. Compared to the active frequency or phase drift methods, the proposed active method can reduce the distortion of grid-current when the inverter works normally. The principles of the islanding detection method based on the feature recognition technology and the improved active method are both analyzed in detail. An 18 kVA DSP-based three-phase inverter with the SVPWM control strategy has been established and tested. Simulation and experimental results verify the theoretical analysis.

Key words: Feature recognition technology, Islanding detection, Non-detection zone, Three-phase inverter system, Voltage harmonic

I. INTRODUCTION

Three-phase grid-connected inverters are an important part of distributed generation systems. An inverter may continue supplying power to a local load when it is disconnected from the grid. In this case, islanding happens and electrical equipment is damaged. As a result, personal safety can be threatened. Therefore, islanding detection is necessary to improve the stability and safety of inverter systems [1]-[6].

Passive islanding detection methods detect the amplitude, frequency, phase angle and harmonic content of the grid voltage. It is easy to realize and does not cause additional current distortion. However, the non-detection zone cannot be avoided [7]-[11]. Active islanding detection methods can reduce the non-detection zones. However, disturbances such as frequency or phase drifts of the grid current are added. The quality of the grid current can be reduced because of these disturbances [12]-[15].

Changes in the parameters of an inverter system can reflect its working condition. If the inverter is disconnected from the grid, some of the parameters may change and can be easily detected. These parameters can be seen as the "features" of the inverter system. The working condition of the system can be recognized depending on these features. Islanding can be detected when these features are changed. As a result, modern feature recognition technology can be introduced to realize islanding detection. Feature recognition contains speaker recognition, image recognition and so on [16]-[20]. Speaker recognition is a typical feature recognition technology. It provides a way to take advantage of speaker features regardless of verbal information [21]. However, it cannot be directly applied to islanding detection. In the Vector Quantization (VQ)-based feature recognition, the decision is made by measuring the similarities between a testing pattern and every codeword achieved during training [22]-[27]. In a three-phase inverter system, the codeword can be seen as the parameters of

Manuscript received May 9, 2015; accepted Nov. 28, 2015
Recommended for publication by Associate Editor Jae-Do Park.
†Corresponding Author: zhengxinin@gmail.com
Tel: +86-0551- 62919033, Fax: +86-0551- 62901135, Hefei University of Technology
*New Energy Automobile Engineering Research Institute, Hefei University of Technology, China

the system, such as the three-phase current and voltage, the DC voltage, the grid frequency, and so on. The codebook is the vector formed by different codewords. A codebook is a collection of codewords which can reflect a certain feature. It can be seen as a feature vector and can be obtained by a theoretical analysis of the inverter's operation condition instead of the training of signals. The codebooks can form an operation vector model of the inverter system. With this model, changes in the features in an inverter system can be detected in real-time.

For the above reasons, a novel islanding detection method based on modern feature recognition technology is proposed in this paper. The features of an inverter system are analyzed. When islanding occurs, one or some of the features change. Abnormal phenomenon can be detected and the non-detection zone can be eliminated. To exacerbate the changes of the features and accelerate the speed of detection, an active islanding detection method is applied. This can help avoid miscalculations. When the grid-connected inverter operates normally, the quality of the grid current is not reduced. When the inverter is disconnected from the grid, the changes in the features can be exacerbated. The operating condition of the inverter will be analyzed in Section II. The vector model will be established and an islanding detection method based on modern feature recognition technology will be introduced in Section III. An active islanding detection method will be described in Section IV. Simulation and experimental results obtained from an 18kVA three-phase grid-connected inverter will be presented to verify the theoretical analysis in Section V.

II. OPERATION ANALYSIS

A. Parameters in the Inverter System

Fig. 1 (a) shows a control diagram of a three-phase grid-connected inverter system. There are several parameters in this system. i_a, i_b and i_c are the AC side current. u_a, u_b and u_c are the AC side voltage. e_a, e_b and e_c are the grid voltage. When the inverter works in the grid-connected condition, u_a, u_b and u_c are the same as e_a, e_b and e_c. θ is the phase angle of the grid voltage, which can be obtained by a PLL. i_d and i_q are the active and reactive current. i_d^* and i_q^* are the references of active and reactive current.

The relationships among the parameters is shown in Fig. 1 (b). When the inverter works in the grid-connected condition, the phase angle of the AC side current is the same as that of the AC side voltage. With the PLL method, a non-ideal grid cannot influence the accuracy of θ [28]-[31]. Therefore, θ can be seen as the ideal value. If u_a, u_b and u_c are sampled, the theoretical values of the AC side current i_a^*, i_b^* and i_c^* and the projection of the three-phase voltage on the dq frame u_d and u_q can be calculated. i_d^* and i_q^* are also the theoretical values of active and reactive current. The actual value of the active and reactive current i_d and i_q can be calculated by i_a, i_b and i_c.

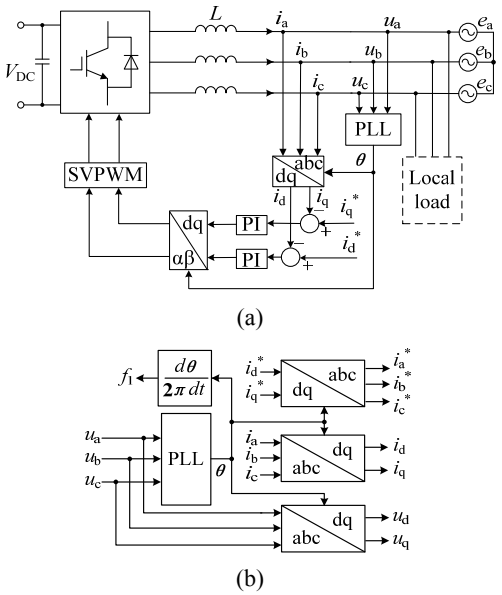

Fig. 1. Introduction of the three-phase inverter system. (a) Control diagram of the system. (b) Relationship among the parameters of the system.

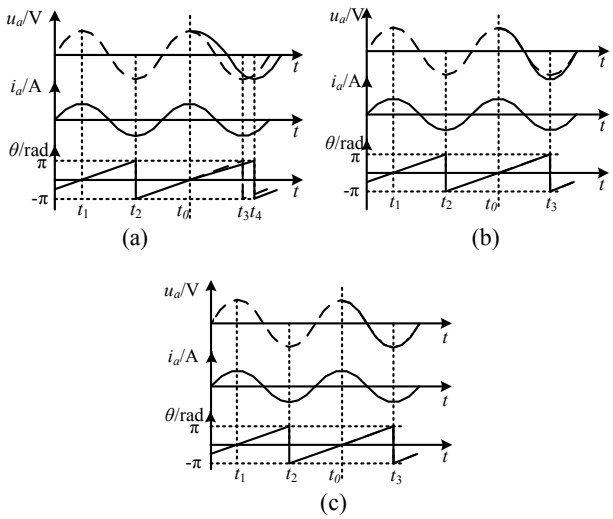

Fig. 2. Changes of the key parameters before and after the inverter is disconnected from the grid. (a) The local load is capacitive or inductive. (b) The local load is resistive without power matching. (c) The local load is resistive with power matching.

The frequency of the grid f_1 can be obtained by a change in the rate of θ.

There are three situations in terms of local loads [32]-[33]. Fig. 2 shows changes in the key parameters before and after the inverter is disconnected from the grid at time t_0. The waveforms from top to bottom are for u_a, i_a and θ. Due to the filter L, the AC side current i_a, i_b and i_c does not have sudden changes. The instantaneous changes at t_0 are not obvious because of the parallel RLC resonant load.

In Fig. 2(a), the local load is capacitive or inductive. Before t_0, the phases of u_a and i_a are the same. θ changes from

–π to π linearly. After t_0, the phases of u_a and i_a are different. θ reaches π at t_4 instead of t_3.

In Fig. 2(b), the local load is resistive and the powers of the load and the inverter are not matched. If the power of the load is lower than that of the inverter, the power of the inverter is partly supply to the grid. If the power of the load is higher than that of the inverter, the power of the load is partly absorbed from the grid. After t_0, the phases of u_a and i_a are still the same. Thus, θ can reach π at t_3. When the inverter is still connected to the grid, the change of θ is the same. However, the amplitude of u_a, u_b and u_c changes, which reflects the change of u_d.

In Fig. 2(c), the local load is resistive and the powers of the load and the inverter are matched. If only the fundamental components are considered, none of the parameters change after t_0. In this condition, a non-detection zone may occur. To avoid this non-detection zone, at least one varying parameter needs to be determined. Therefore, further analysis is necessary.

B. Changes in the Parameters

To avoid a non-detection zone, only the third situation is under consideration. When the inverter is connected to the grid, u_d is regulated according to standards. It is limited in a certain range. The voltage harmonics are also regulated according to standards and their content is slight. After the inverter is disconnected from the grid, u_a, u_b and u_c are not clamped by the grid voltage. The harmonics of u_a, u_b and u_c increase because of the switching and nonlinear load.

The voltage harmonics introduced by the switching are caused by two reasons [34]. One is dead-time. The other is SVPWM (Space Vector Pulse Width Modulation). The output voltage harmonic of the bridge arm caused by the dead-time can be expressed as:

$$u_{oh(td)} = -\frac{4V_{DC}}{\pi h}\frac{t_d}{T_c}\sin h\omega_1 t \tag{1}$$

where t_d is the dead-time and T_c is the switching cycle. The output voltage harmonic of the bridge leg caused by the SVPWM can be expressed as:

$$u_{oh(sw)} = C_{mn}\cos h\omega_1 t \tag{2}$$

where n corresponds to the multiple of the reference wave frequency, and m corresponds to the multiple of the carrier wave frequency. h is $m*(f_c/f_1)+n$. The coefficient C_{mn} can be expressed as:

$$C_{mn} = A_{mn} + jB_{mn} = \frac{1}{2\pi^2}\int_{-\pi}^{\pi}\int_{-\frac{\pi[1+u_{\mathrm{mod}}(y)]}{2V_{DC}}}^{\frac{\pi[1+u_{\mathrm{mod}}(y)]}{2V_{DC}}} V_{DC}e^{j(mx+ny)}dxdy \tag{3}$$

The equivalent reference of the SVPWM control u_{mod} can be expressed as:

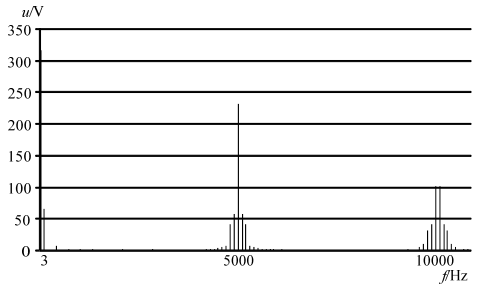

Fig. 3. Voltage harmonics of the bridge leg caused by SVPWM.

$$u_{\mathrm{mod}} = \frac{MV_{DC}}{2}\cos\omega_1 t - \frac{MV_{DC}}{2}[\frac{\sqrt{3}}{2}\cos(\omega_1 t - \frac{k\pi}{3} + \frac{\pi}{6}) - \begin{cases}\cos(\omega_1 t - \frac{k\pi}{3}) & k = 1,3,5\\ \cos(\omega_1 t - \frac{k\pi}{3} + \frac{\pi}{6}) & k = 2,4,6\end{cases}] \tag{4}$$

where V_{DC} is the DC voltage, M is the modulation ratio, and k is the sector number. At a low frequency, m is 0, and n is a multiple of 3.

Fig. 3 shows the voltage harmonics of the bridge leg caused by the SVPWM. The switching frequency f_s is 5kHz. The grid current can be seen as the superposition of the fundamental current and the harmonics. The local load can be simplified as a parallel circuit of the resistor R_l, the inductor L_l and the capacitor C_l. The resonance frequency can be expressed as:

$$f_r = \frac{1}{2\pi\sqrt{L_l C_l}} \tag{5}$$

When f_r is the grid frequency f_1, the local load is resistive. If the inverter is disconnected from the grid, the current harmonics caused by the voltage harmonics u_{oh} described in (1) and (2) can be expressed as:

$$i_h = u_{oh}/(\frac{jh\omega_1 R_l L_l}{jh\omega_1 R_l C_l + h^2\omega_1^2 C_l L_l + 1} + jh\omega_1 L) \tag{6}$$

where L is the AC side filter. Thus, the AC side voltage can be expressed as:

$$u_h = u_{oh}\frac{R_l L_l}{R_l L_l + h^2\omega_1^2 C_l L_l L + L + jh\omega_1 R_l C_l L} \tag{7}$$

The voltage harmonic projections in the dq-frame can be expressed as:

$$\begin{bmatrix}u_{d(h\pm1)}\\ u_{q(h\pm1)}\\ 0\end{bmatrix} = \frac{2}{3}\begin{bmatrix}\cos\omega_1 t & \cos(\omega_1 t - \frac{2\pi}{3}) & \cos(\omega_1 t + \frac{2\pi}{3})\\ -\sin\omega_1 t & -\sin(\omega_1 t - \frac{2\pi}{3}) & -\sin(\omega_1 t + \frac{2\pi}{3})\\ \frac{1}{2} & \frac{1}{2} & \frac{1}{2}\end{bmatrix}\begin{bmatrix}u_{ah}\\ u_{bh}\\ u_{ch}\end{bmatrix} \tag{8}$$

Fig. 4 shows the changes in the AC side voltage caused by the SVPWM. The inverter is disconnected from the grid at the time t_0. The switching frequency current harmonic is added to the ideal fundamental current of the AC side.

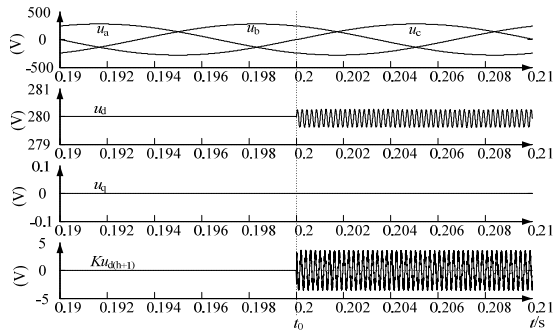

Fig. 4. Changes of the AC side voltage caused by SVPWM.

The top waveforms u_a, u_b and u_c do not noticeably change after t_0. u_d and u_q are the projections of u_a, u_b and u_c in the dq-frame. The phase angle, which takes part in the coordinate transformation, is the output of the PLL. The input of the PLL is u_a, u_b and u_c so that u_q is always 0. The frequency of the three-phase current harmonic is the switching frequency f_s. The bottom waveform $Ku_{d(h+1)}$ is the output of a high passed filter (HPF). The input of the HPF is u_d. K is the gain of the HPF. In order to amplify the voltage harmonic, K is set as 10 in this paper. h is the voltage harmonic order, which is f_s/f_1. The cut-off frequency of the HPF should be less than f_s. It is set as 2.5kHz in this paper. The voltage harmonic noticeably changes after t_0. Thus, the non-detection zone can be solved through testing u_{dh} by a HPF.

The voltage harmonics introduced by the nonlinear load also contain the low and high frequency components [35]. After the inverter is disconnected from the grid, the voltage harmonics with both low and high frequencies increase. The delay of the HPF is much shorter than that of a LPF (Low Passed Filter). Therefore, a HPF is applied instead of other filters.

III. Model Islanding Detection Method

A. Establishment of a Vector Model

Changes in the parameters are analyzed in Section II. Thus, the features of the inverter system can be extracted. The feature vector can be expressed as:

$$\boldsymbol{Y} = \{\boldsymbol{y}_1, \boldsymbol{y}_2\} \tag{6}$$

$\boldsymbol{y}_1$ and $\boldsymbol{y}_2$ are two groups of three-dimensional vectors. They can be expressed as:

$$\boldsymbol{y}_1 = [i_a, i_b, i_c]^T \tag{7}$$

$$\boldsymbol{y}_2 = [f_1, u_d, f(u_{dh})]^T \tag{8}$$

$\boldsymbol{y}_1$ is a feature of the current in an inverter system, and $\boldsymbol{y}_2$ is a feature of the voltage. u_{dh} is a sinusoidal variation and cannot be applied in the feature recognition as a codeword. It can be replaced by a function $f(u_{dh})$, which is the amplitude of u_{dh}. The algorithm of $f(u_{dh})$ is shown in Fig. 5.

In Fig. 5, f_z is the testing frequency of u_{dh}. The calculation of $f(u_{dh})$ costs half of a switching cycle, which is a very short time.

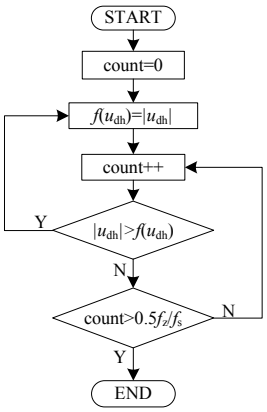

Fig. 5. The algorithm of $f(u_{dh})$.

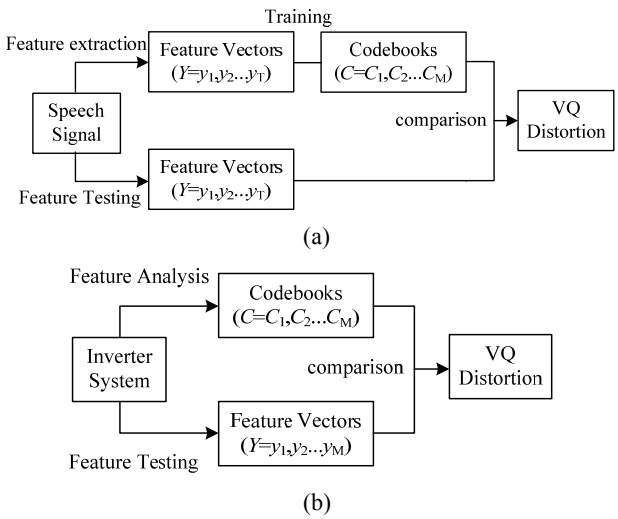

Fig. 6. Comparison of the processes of the speaker recognition and the islanding detection method. (a) The speaker recognition. (b) The islanding detection method.

B. Islanding Detection Method

The theoretical value of the feature vector can be expressed as:

$$\boldsymbol{C}_1 = [i_a^*, i_b^*, i_c^*]^T \tag{9}$$

$$\boldsymbol{C}_2 = [f_1^*, u_d^*, f(u_{dh}^*)]^T \tag{10}$$

where $\boldsymbol{C}_1$ and $\boldsymbol{C}_2$ are the codebooks. i_a^*, i_b^*, i_c^*, f_1^*, u_d^* and $f(u_{dh}^*)$ are the codewords. $f(u_{dh}^*)$ is 0 in the ideal condition.

According to standard GB12325-90, the ideal value of f_1^* is 50Hz, and u_d^* is 280V. A slight deviation is allowed in the standard. Therefore, $\boldsymbol{C}_1$ and $\boldsymbol{C}_2$ are different from $\boldsymbol{y}_1$ and $\boldsymbol{y}_2$ even when the inverter works normally. Therefore, islanding should be judged by the mean square quantization distortion, which can be expressed as:

$$d = \sum_{i=1}^{2} d_i = \sum_{i=1}^{2}\sum_{j=1}^{3} \alpha_{ij}(y_{ij} - C_{ij})^2 \tag{11}$$

The threshold δ should be set reasonably set. When the inverter works normally, δ should be larger than d. When the

inverter is disconnected from the grid, d exceeds δ and islanding can be detected. δ can be expressed as:

$$\delta = \sum_{i=1}^{2}\sum_{j=1}^{3}\alpha_{ij}(C_{ij\max} - C_{ij\min})^2 \tag{12}$$

where C_{ijmax} and C_{ijmin} are the upper and lower limits of the codewords regulated by standards. Fig. 6 shows the processes of the speaker recognition and the proposed islanding detection method. It can be seen that the codebooks of the islanding detection method can be directly obtained by the feature analysis, while the codebooks of the speaker recognition are obtained by Vector Quantization.

IV. Active Detection Method

If an inverter is connected to a non-ideal grid, voltage harmonics always occur and u_{dh} in Fig. 5 is not zero before t_0. Islanding may be misjudged through testing $f(u_{dh})$ if the threshold δ is too small. However, the changes in the features may be slight. If δ is too high, islanding may not be detected in time. To accelerate the speed of detection and to avoid miscalculation, an active islanding detection method should be applied to exacerbate the changes in the features. According to the above analysis, after the inverter is disconnected from the grid, u_d cannot be clamped by the grid. If a disturbance is added to exacerbate the changes in u_d, islanding can be easily detected. Fig. 7 shows an active islanding detection method.

$f(u_{dh})$ described in Fig. 5 is added to the active current reference i_d^*. A HPF is applied to separate the high frequency voltage harmonics. u_{dh} is the output of the HPF, which was designed in section II. It is the sum of the high frequency voltage harmonics. Their frequencies are higher than the cut-off frequency of the HPF.

In a non-ideal grid, the grid harmonics are mainly the 3rd, 5th, 7th, 11th and 13th time voltage harmonics [36]. The containing of the switching frequency voltage harmonics is very slight. Therefore, $f(u_{dh})$ is close to 0 when the inverter connects to the grid. If islanding happens, the AC side voltage is not be clamped by the grid and $f(u_{dh})$ increases. According to the current loop shown in Fig. 8, u_{oh} increases with an increment of $f(u_{dh})$. According to (7) and (8), $f(u_{dh})$ increases further. After a few times' accumulation, the islanding can be quickly detected.

V. Simulation and Experimental Results

An 18kVA three-phase grid-connected inverter with the SVPWM control method has been simulated by the simulation software MATLAB/Simulink. The grid is 220V/380V/50Hz, and the DC voltage is 700V.

Fig. 9 shows the changes in the parameters both with and without the active islanding detection method. The

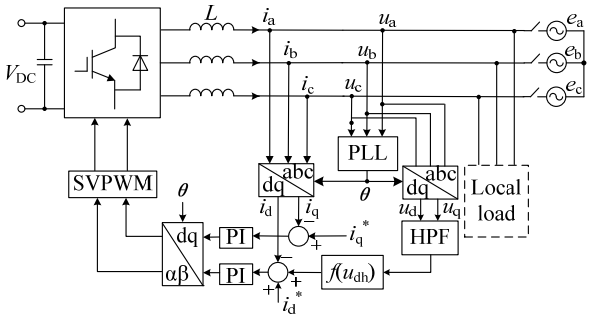

Fig. 7. Active islanding detection method.

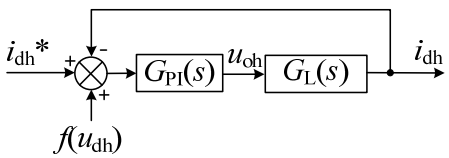

Fig. 8. Control diagram of the current loop.

three-phase inverter is simulated by a three-phase current source. The amplitude of the fundamental current is 40A. The amplitude of the switching frequency positive sequence current harmonic is 1A. The switching frequency f_s is 5kHz. The RLC resonant load is 7Ω, 10.1424mH and 1000μF. The resonant frequency of the local load is 50Hz. The parameters of the HPF are the same as those from the theoretical analysis.

The inverter is disconnected from the grid at time t_0. Fig. 9 (a) shows the AC side voltage and current without the active islanding detection method. It seems that there is no change and that islanding can happen. However, the parameters discussed in Section III change obviously after t_0.

In Fig. 9 (b), the waveforms from top to bottom respectively are u_d, u_{dh} and $f(u_{dh})$. Positive sequence current harmonics are added so that h is f_s/f_1+1 in this figure. According to $f(u_{dh})$, islanding can be detected.

Fig. 9 (c) shows the AC side voltage and current with the active islanding detection method. The AC side voltage and current change obviously after the inverter is disconnected from the grid. Because of the positive feedback, the amplitude of the current harmonic is able to increase after t_0, which is shown in Fig. 9 (d). Thus, the islanding can be quickly detected.

Tab. 1 shows the values of the parameters of (12). The principle of the weighting factors α_{ij} is that the influence of the parameters can realize an average distribution. According to Tab. 1, the threshold δ can be set as 1.

Fig. 10 shows the passive and active islanding detection results in a non-ideal grid. An 18kVA three-phase inverter model is applied. The waveforms from top to bottom are the AC side voltage u_a, u_b and u_c, the AC side current i_a, i_b and i_c, the driving enable signal, d and δ. The inverter is disconnected from the grid at the time t=0.04s.

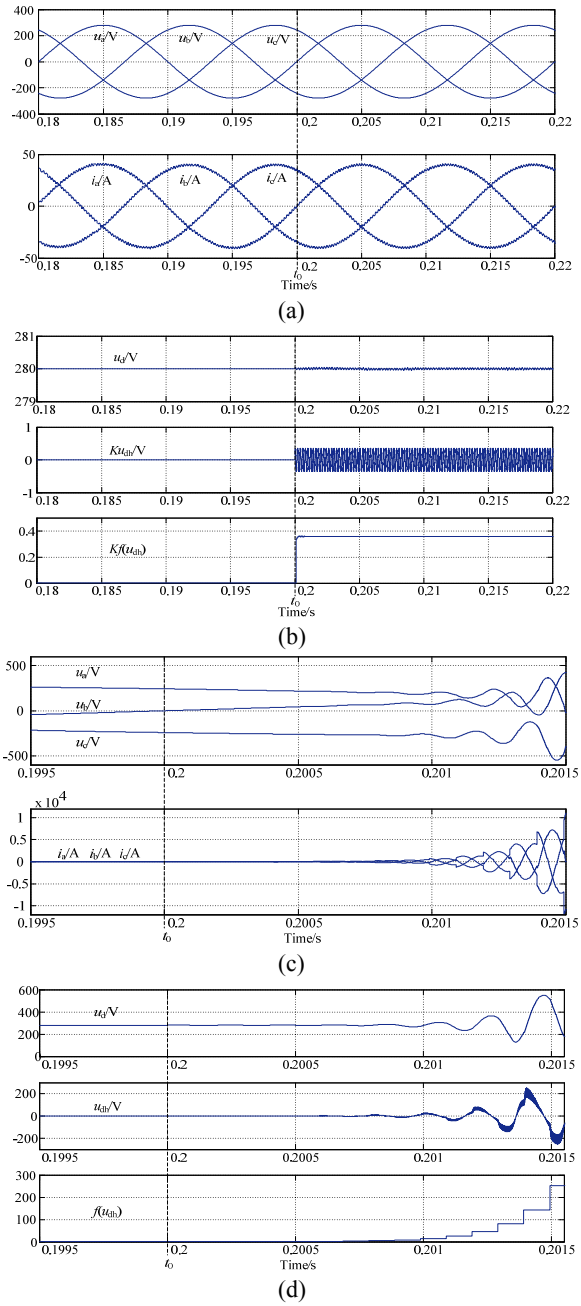

Fig. 9. Changes of the parameters. (a) AC side voltage and current without active islanding detection method. (b) The feature parameters without active islanding detection method. (c) AC side voltage and current with active islanding detection method. (d) The feature parameters with active islanding detection method.

TABLE I
THE VALUES OF THE PARAMETERS

i	j	α_{ij}	C_{ijmax}	C_{ijmin}
1	1	0.03	30	24.5
1	2	0.03	30	24.5
1	3	0.03	30	24.5
2	1	0.17	50.5	49.5
2	2	0.0015	336	224
2	3	0.6	0.28	0

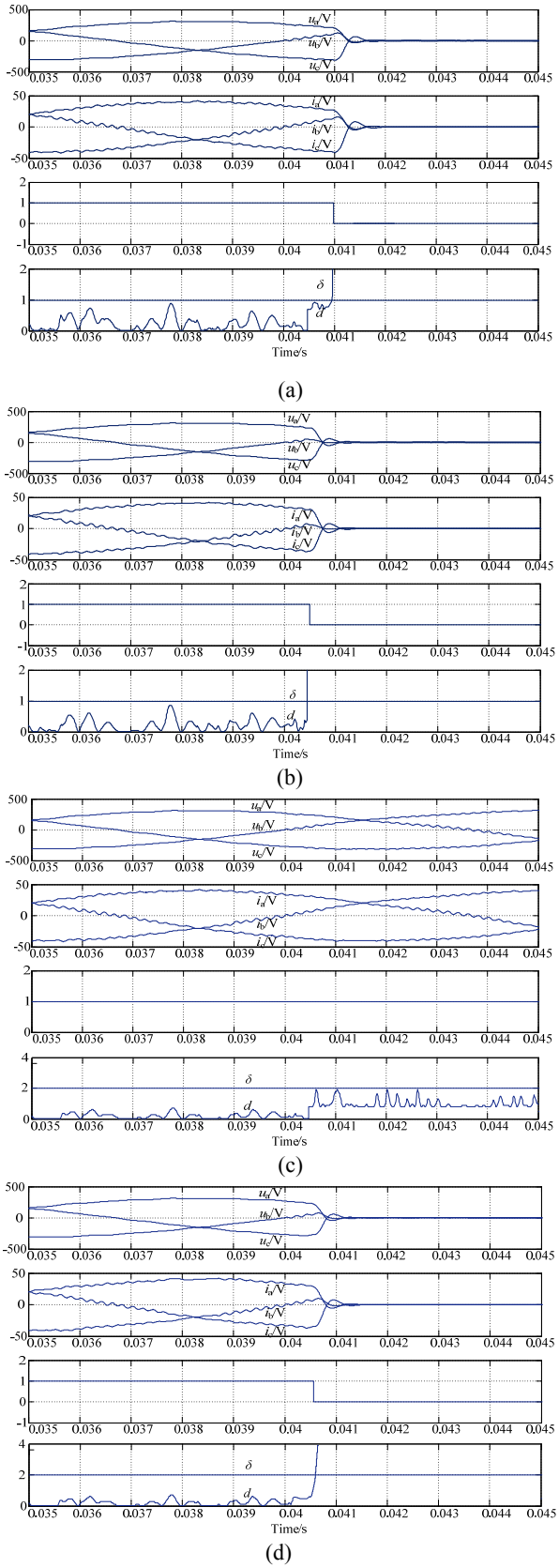

Fig. 10. The islanding detection result in the non-ideal grid. (a) Passive islanding detection method (δ=1). (b) Active islanding detection method (δ=1). (c) Passive islanding detection method (δ=2). (d) Active islanding detection method (δ=2).

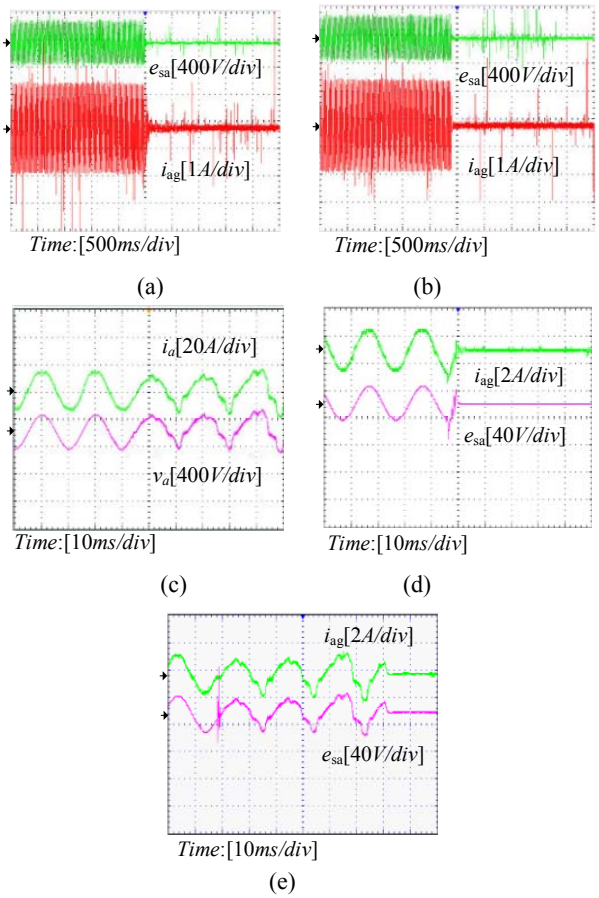

Fig. 11. Experimental results in the non-ideal grid. (a) Passive islanding detection method (δ=1). (b) Active islanding detection method (δ=1). (c) Passive islanding detection method (δ=2). (d) Active islanding detection method (δ=2). (e) AFD islanding detection method.

Fig. 10(a) and (b) show the passive and active islanding detection results when the threshold δ is 1. The islanding is more quickly detected with the active islanding detection method. However, sometimes d is close to δ when the inverter works normally. δ should be high enough to avoid misprotection. However, it cannot be too high to detect the islanding. Fig. 10(c) and (d) show the detection results when δ is 2. The islanding may not be detected with the passive islanding detection method while the active islanding detection method can solve the problem.

An 18kVA three-phase grid-connected inverter with the SVPWM control strategy based on a TMS320F240PQA has been built to verify the analysis. The parameters are the same as those used in the simulation.

Fig. 11(a) and (b) show the experimental results with the passive and active islanding detection method when δ is 1. The waveforms from top to the bottom are the AC side voltage u_a, u_b and u_c, and the AC side current i_a, i_b and i_c. The islanding can be quickly detected with both methods.

Fig. 11(c) and (d) show the experimental results when δ is 2. The islanding can be quickly detected with the active method. However, the passive method cannot detect the islanding in time. Fig. 11 (e) shows the experimental results with the active frequency drift (AFD) method. The detection speed of the proposed active detection method is quicker than that of the AFD method.

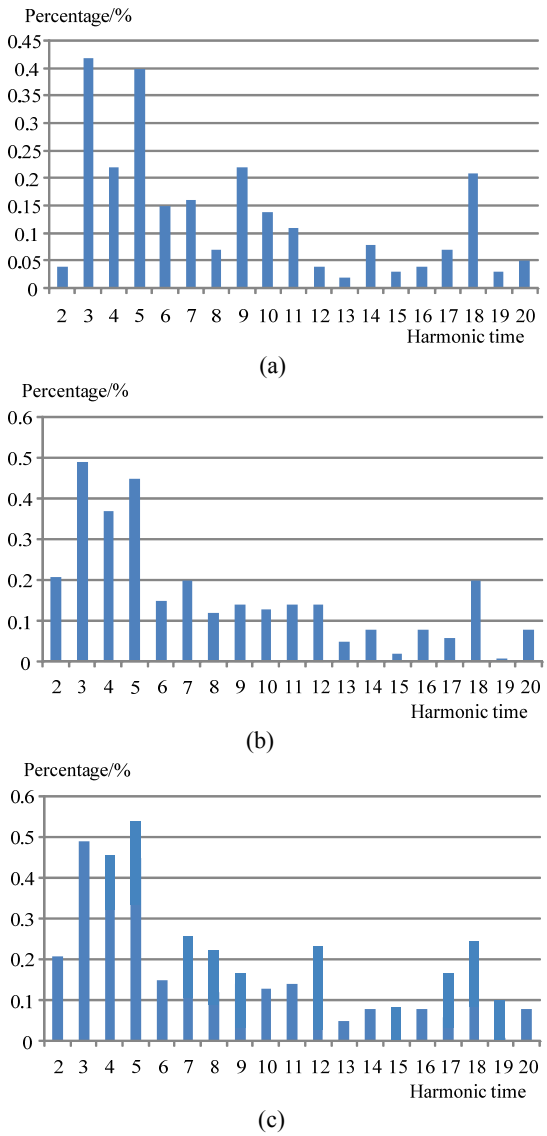

Fig. 12. The current harmonics. (a) Passive islanding detection method. (b) Active islanding detection method. (c) Active islanding detection method.

Fig. 12 shows the current harmonics of the grid current when the inverter works normally. There are third-time current harmonics because the three-phase transformer is not completely symmetrical. Fig. 12 (a) and (b) are the current harmonics with the passive and active islanding detection methods. Their THDs are 3.7 and 4.0, respectively. It can be seen that the active islanding detection method does not introduce a lot of harmonic. The lower h is, the higher the increment of the current harmonic becomes. Fig. 12 (c) shows the current harmonics with the AFD. The THD is 4.9 and it is higher than that of the proposed method.

VI. Conclusion

This paper proposes a novel islanding detection method based on the modern feature recognition technology. The proposed method can identify the features of the inverter system and it can calculate the quantizing distortion. The principle of the feature recognition technology is described in detail. Passive and active islanding detection methods based on feature recognition technology are analyzed. Simulation and experimental results from an 18 kVA grid-connected inverter are presented to verify the theoretical analysis. The proposed method has the following advantages:

1) This method can avoid the non-detection zone through changes of the parameters.

2) The active method can accelerate the speed of detection and avoid miscalculation.

3) Compared to the active frequency or phase drift methods, the AC side current with the proposed method has less distortion when the inverter works normally.

Acknowledgment

The authors would like to acknowledge the support provided by the Special Foundation for doctoral degree (JZ2015HGBZ0456), the National Natural Science Foundation (51377082), and the "Blue Project" project in Jiangsu Province.

References

[1] D. Reigosa, F. Briz, C. Blanco, P. Garcia, and J. M. Guerrero, "Active islanding detection for multiple parallel-connected inverter-based distributed generators using high-frequency signal injection," *IEEE Trans. Power Electron.*, Vol. 29, No. 3, pp. 1192-1199, Mar. 2014.

[2] D. Zhang, H. C. Niu, and M. Jiang, "Modeling of islanding detection by sensing jump change of harmonic voltage at PCC by the combination of a narrow band-pass filter and wavelet analysis," in *IEEE ECCE Asia Downunder*, pp. 1289-1294, Jun. 2013.

[3] W. Cai, B. Liu, S. Duan, and C. Zou, "An islanding detection method based on dual-frequency harmonic current injection under grid impedance unbalanced condition," *IEEE Trans. Ind. Informat*., Vol. 9, No. 2, pp. 1178-1187, May 2013.

[4] E. J. Estébanez, V. M. Moreno, A. Pigazo, M. Liserre, and A. Dell'Aquila, "Performance evaluation of active islanding-detection algorithms in distributed-generation photovoltaic systems: two inverters case," *IEEE Trans. Ind. Electron*., Vol. 58, No. 4, pp. 1185-1193, Apr. 2011.

[5] S. H. Lee and J.-W. Park, "Improvement on stability and islanding detection performances by advanced inverter control of DG," *IEEE Trans. Power Syst*., Vol. 28, No. 4, pp. 3954-3963, Nov. 2013.

[6] R. M. Kamel, A. Chaouachi, and K. Nagasaka, "Three control strategies to improve the microgrid transient dynamic response during isolated mode: a comparative study," *IEEE Trans. Ind. Electron*., Vol. 60, No. 4, pp. 1314-1322, Apr. 2013.

[7] G. G. Pozzebon, A. F. Q. Goncalves, G. G. Pena, N.E.M. Mocambique, and R. Q. Machado, "Operation of a three-Phase power converter connected to a distribution system," *IEEE Trans. Ind. Electron*., Vol. 60, No. 5, pp. 1810-1818, May 2013.

[8] H. Laaksonen, "Advanced islanding detection functionality for future electricity distribution networks," *IEEE Trans. Power Del*., Vol. 28, No. 4, pp. 2056-2064, Oct. 2013.

[9] H. Vahedi, G. B. Gharehpetian, and M. Karrari, "Application of duffing oscillators for passive islanding detection of inverter-based distributed generation units," *IEEE Trans. Power Del*., Vol. 27, No. 4, pp. 1973-1983, Oct. 2012.

[10] J.-H. Kim, J.-G. Kim, Y.-H. Ji, Y.-C. Jung, and C.-Y. Won, "An islanding detection method for a grid-connected system based on the goertzel algorithm," *IEEE Trans. Power Electron.,* Vol. 26, No. 4, pp. 1049-1055, Apr. 2011.

[11] A. Cataliotti, V. Cosentino, N. Ngoctrung, and P. Russotto, "Hybrid passive and communications-based methods for islanding detection in medium and low voltage smart grids," in *4th International Power Engineering, Energy and Electrical Drives(POWERENG)*, pp. 1563-1567, May 2013.

[12] A. Yafaoui, B. Wu, and S. Kouro, "Improved active frequency drift anti-islanding detection method for grid connected photovoltaic systems," *IEEE Trans. Power Electron.,* Vol. 27, No. 5, pp. 2367-2375, May 2012.

[13] H. H. Zeineldin and M. M. A. Salama, "Impact of load frequency dependence on the NDZ and performance of the SFS islanding detection method," *IEEE Trans. Ind. Electron.*, Vol. 58, No. 1, pp. 139-146, Jan. 2011.

[14] Q. Zhang, X. Sun, Y. Zhong, B. Ren, and M. Matsui, "Research on an novel active anti-islanding method based on positive feedback of even harmonic current disturbance," in *IEEE Power Engineering and Automation Conference (PEAM)*, pp. 22-25, Sep. 2011.

[15] H. Novanda, P. Regulski, V. Stanojevic, and V. Terzija, "Assessment of frequency and harmonic distortions during wind farm rejection test," *IEEE Trans. Sustain. Energy*, Vol. 4, No. 3, pp. 698-705, Jul. 2013.

[16] M. Ferras and H. Bourlard, "MLP-based factor analysis for tandem speech recognition," in *IEEE International Conference on Acoustics, Speech and Signal Processing (ICASSP)*, pp. 6719-6723, May 2013.

[17] J. Ming, R. Srinivasan, D. Crookes, and A. Jafari, "CLOSE—a data-driven approach to speech separation," *IEEE Trans. Audio, Speech, Language Process*., Vol. 21, No. 7, pp. 1355-1368, Jul. 2013.

[18] S. Garimella and H. Hermansky, "Factor analysis of auto-associative neural networks with application in speaker verification," *IEEE Trans. Neural Netw. Learn. Syst.,* Vol. 24, No. 4, pp. 522-528, Apr. 2013.

[19] Y.-T. Chuang, Y.-L. Hong, K.-C. Huang, and S.-W. Shih, "Autofocus of iris patterns using a triangle aperture," *IEEE Trans. Cybern*., Vol. 43, No. 4, pp. 1304-1309, Aug. 2013.

[20] M. Hu, Y. Wang, Z. Zhang, D. Zhang, and J. J. Little, "Incremental learning for video-based gait recognition with LBP flow," *IEEE Trans. Cybern*., Vol. 43, No. 1, pp. 77-89, Feb. 2013.

[21] T. Kinnunen, E. Karpov, and P. Franti, "Real-time speaker identification and verification," *IEEE Trans. Audio, Speech, Language Process*., Vol. 14, No. 1, pp. 277-288, Jan. 2006.

[22] B. V. Srinivasan, Y. Luo, D. G. Romero, D. N. Zotkin, and R. Duraiswami, "A symmetric kernel partial least squares framework for speaker recognition," *IEEE Trans. Audio, Speech, Language Process*., Vol. 21, No. 7, pp. 1415-1423, Jul. 2013.

[23] L. E. Shafey, C. Mccool, R. Wallace, and S. Marcel, "A

scalable formulation of probabilistic linear discriminant analysis: applied to face recognition," *IEEE Trans. Pattern Anal. Mach. Intell.,* Vol. 35, No. 7, pp. 1788-1794, Jul. 2013.
[24] S. Yaman and J. Pelecanos, "Using polynomial kernel support vector machines for speaker verification," *IEEE Signal Process. Lett.,* Vol. 20, No. 9, pp. 901-904, Sep. 2013.
[25] W. Rao and M.-W. Mak, "Boosting the performance of i-vector based speaker verification via utterance partitioning," *IEEE Trans. Audio, Speech, Language Process*., Vol. 21, No. 5, pp. 1012-1022, May 2013.
[26] R. Wallace and M. McLaren, "Total variability modelling for face verification," *IET Biometrics*, Vol. 1, No. 4, pp. 188-199, Dec. 2012.
[27] M. S. Paja, T. H. Falk, and D. O'Shaughnessy, "Whispered speaker verification and gender detection using weighted instantaneous frequencies," in *IEEE International Conference on Acoustics, Speech and Signal Processing (ICASSP)*, pp. 7209-7213, May 2013.
[28] S. A. O. Silva, R. Novochadlo, and R. A. Modesto, "Single-phase PLL structure using modified p-q theory for utility connected systems," in *IEEE Power Electronics Specialists Conference(PESC)*, pp. 4706-4711, Jun. 2008.
[29] C. H. G. Santos, S. M. Silva, and B. J. C. Filho, "A fourier-based PLL for Single-Phase grid connected systems," in IEEE Energy Conversion Congress and Exposition(ECCE), pp. 2626-2632, Sep. 2010.
[30] K.-J. Lee, J.-P. Lee, D. Shin, D.-W. Yoo, and H.-J. Kim, "A novel grid synchronization PLL method based on adaptive low-pass notch filter for grid-connected PCS," *IEEE Trans. Ind. Electron.*, Vol. 61, No. 1, pp. 292-301, Jan. 2014.
[31] M. K. Ghartemani, S. A. Khajehoddin, P. K. Jain, and A. Bakhshai, "Problems of startup and phase jumps in PLL systems," *IEEE Trans. Power Electron*., Vol. 27, No. 4, pp. 1830-1838, Apr. 2012.
[32] J. He and Y. W. Li, "Hybrid voltage and current control approach for DG-grid interfacing converters with LCL filters," *IEEE Trans. Ind. Electron*., Vol. 60, No. 5, pp. 1797-1809, May 2013.
[33] S. Mishra, D. Ramasubramanian, and P. C. Sekhar, "A seamless control methodology for a grid connected and isolated PV-diesel microgrid," *IEEE Trans. Power Syst*., Vol. 28, No. 4, pp. 4393-4404, Nov. 2013.
[34] J. Li, J. Li, and S. Ding, "Research on a novel method for improving inverter output waveforms," in 5th IEEE Conference on Industrial Electronics and Applications (ICIEA), pp. 1194-1197, Jun. 2010.
[35] B. Singh, K. A. Haddad, and A. Chandra, "Harmonic elimination, reactive power compensation and load balancing in three-phase, four-wire electric distribution systems supplying non-linear loads," *Electric Power Systems Research*, Vol. 44, No. 2, pp. 93-100. Feb. 1998.
[36] J. Lianwei, D. Qinhua, and Z. Jiang, "Harmonic survey and solutions of Xining power grid in western China," in *International Conference on Power System Technology*, pp. 1161-1165, Dec. 2000.

Xinxin Zheng was born in Anhui, China. She received her B.S. and Ph.D. degrees in Electrical Engineering from the Nanjing University of Aeronautics and Astronautics, Nanjing, China, in 2009 and 2015, respectively. She is presently working in the New Energy Automobile Engineering Research Institute, Hefei University of Technology, Hefei, China. Her current research interests include islanding detection methods and feature recognition technology.

Lan Xiao was born in Zhejiang, China. She received her B.S. and Ph.D. degrees in Electrical Engineering from the Nanjing University of Aeronautics and Astronautics (NUAA), Nanjing, China, in 1993 and 1998, respectively. In 1999, she joined the faculty of the College of Automation Engineering, NUAA. She is presently working as a Professor at the Aero-Power SCI Tech-Center, NUAA. She is the author or co-author of more than 50 technical papers in journals and conferences proccedings.

Wenwen Qin was born in Anhui, China, in 1989. He received his B.S. degree in Electrical Engineering from the Hefei University of Technology, Anhui, China, in 2014; where he is presently working towards his M.S. degree. His current research interests include battery management systems, wireless charging of EVs, and the design of AC-DC and DC-DC controllers.

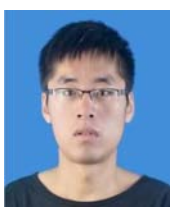

Qing Zhang was born in China, in 1990. He received his B.S. degree in Automation from Hefei University of Technology, Anhui, China, in 2014; where he is presently working towards his M.S. degree. His current research interests include battery management systems, automatic control and wireless charging of EVs.